Semiclassical and microscopic calculations of the spin-orbit density part of the Skyrme nucleus-nucleus interaction potential with temperature effects included

Raj K. Gupta,[1,2] Dalip Singh,[1,2] and Walter Greiner[2]

[1]*Department of Physics, Panjab University, Chandigarh-160014, India*

[2]*Frankfurt Institute for Advanced Studies (FIAS), Johann Wolfgang Goethe-Universität, Max-von-Laue-Str. 1,*
D-60438 Frankfurt am Main, Germany

The semiclassical formulation of the Skyrme energy density functional for spin-orbit density part of the interaction potential is compared with the microscopic shell model formulation, at both the ground state and finite temperatures. The semiclassical spin-orbit interaction potential is shown to contain exactly the same shell effects as are there in the microscopic shell model, provided a normalization of all semiclassical results to the spin-saturated case (for one or both nuclei as spin-saturated) is made. On the other hand, the α nucleus structure present in microscopic shell model is found absent in semiclassical approach. The role of temperature is found not to change the behavior of shell or α nucleus structure effects up to about 3 MeV, and increase or decrease the height of the (normalized) barriers in accordance with the shell structure of nuclei. Calculations are made for three two-nucleon transfer reactions forming the α-nucleus $A = 4n$, $N = Z$ compound systems ^{56}Ni* and ^{48}Cr* and the non-α-nucleus compound system ^{52}Cr*, and for Skyrme forces SIII and SLy4. The two parameter Fermi density, with its parameters fitted to experiments and made temperature dependent in a model way, is used for the nuclear density in semiclassical calculations, and the same in microscopic shell model is achieved via the Fermi-Dirac occupation of shell model states and particle number conservation.

I. INTRODUCTION

In the recent past, in a series of papers [1–10], one of us (R.K.G.) and Collaborators studied the role of the spin-orbit density part of the interaction potential in Skyrme energy density formalism [11] and proposed a simple analytical formulation of the potential, for both the spin-orbit density independent part and the spin-orbit density term itself, respectively, as the proximity potential and in terms of the masses of colliding nuclei and their associated particle strength which accounts for the shell structure effects via the number of valence particles outside the closed core. The role of spin-orbit density part of the interaction potential is shown to be important, not only for its significant contribution to fusion cross sections [5], but also for the α-nucleus structure of colliding $N = Z$, α-nuclei and its suppression for colliding non-α nuclei [9]. Considering a two-nucleon transfer process, it is shown that the α-particle transfer is related to the closure of the last j shell for both the protons and neutrons of at least one of the product nuclei. This is manifested as a discontinuity (a definite step) in the barriers, as well as in the transfer yields, at the α-nucleus transfer products. Closed shells, but no discontinuities, are also found for two-nucleon transfer products, but then the closed j shell occurs for either the protons or neutrons and not for both protons and neutrons. For non-α colliding nuclei, the discontinuities in potentials and yields occur also at two nucleon transfer products, irrespective of the above noted shell closure effects. The same α-nucleus structure effect is found to exist for the valence particles number and/or weighted valence particles number, called particle strength, and hence is a representation of shell effects in spin-orbit density part of the interaction potential. The simple analytical formulas provided a unique possibility to replace the time consuming microscopic

theoretical calculations, and for making predictions of fusion cross sections, including for exotic neutron-rich colliding nuclei [12–14]. The microscopic calculations of the spin-orbit density part of Skyrme nucleus-nucleus interaction potential were made for both the shell model (SM) densities and two-parameter Fermi densities, yielding nearly the same result.

More recently, an alternative to help reduce the lengthy microscopic calculations is provided by the semiclassical formulation of the Skyrme energy density functional. The semiclassical method of expansions, with $\hbar$ as the order parameter, worked out in the framework of extended Thomas-Fermi (ETF) model has been very successful, which expresses the kinetic energy density τ and spin-orbit density $\vec{J}$ as functions of the nucleon density $\rho(\vec{r})$ [15–18], used in self-consistent variational approach with nucleon densities as the variational quantities. Thus, the Skyrme energy density becomes a functional of the nucleon densities alone, and hence eliminates completely the use of single particle wave functions. The (variational) nucleon densities are taken as the Hartree-Fock (HF) densities, Hartee-Fock-Bogoliubov (HFB) densities, or simply the modified (two-parameter) Fermi density with an additional parameter [17–21]. Some effort has gone in to comparing the results of semiclassical calculations using modified Fermi densities with ones using HF densities (or the two densities themselves) [18,20], but so far *no* calculation seems to have been made to compare the semiclassical approach with the microscopic shell model approach introduced by Vautherin and Brink [11] for spherical (doubly closed shell) nuclei and by one of us (R.K.G.) and Collaborators [1] for unclosed shell nuclei, in particular for the spin-orbit density term in Skyrme energy density functional. The use of microscopic shell model wavefunctions reduce the angular variables in

Hartree-Fock equations, such that the densities $\rho(\vec{r})$, $\tau(\vec{r})$, and (the modulus of) $\vec{J}(\vec{r})$ depend on the radial coordinate r only. We make such a comparison between the semiclassical and the microscopic shell model approaches here in this paper for the spin-orbit interaction potential and for transfer reactions. Note that in transfer reactions a spin-saturated target-projectile combination such as ^{16}O+^{40}Ca (nuclei with major shell closed for both protons and neutrons) would become spin-unsaturated ones like ^{18}Ne+^{38}Ar, ^{20}Ne+^{36}Ar, etc., with valence particle configurations. Furthermore, in microscopic shell model approach the spin-orbit density is zero ($\vec{J}_q = 0$; $q = n$ or p) for nuclei with major shells completely filled, which is not the case in semiclassical approach since it depends only on nucleon density. This later observation makes the comparison between microscopic shell model and semiclassical results more meaningful and interesting.

Semiclassical ETF approach is also extended to nuclear systems at finite temperatures [17,22], but for the free energy and entropy density functionals only. For the spin-orbit density functional $\vec{J}(\rho)$ of the semiclassical formalism, we include the temperature effects here in the following via the nuclear density, taken as the two-parameter Fermi density [23]. This follows from the fact that at higher temperatures the HF density takes nearly a shape of Fermi-type, i.e., become flat in the interior region of small r-values [24]. Furthermore, the Fermi density distributions and shell model density distributions, as well as the spin-orbit density interaction potentials based on them, are found to be nearly the same [1,4,7], at least in the surface region of relevance for heavy ion collisions. Hence, we compare the above-mentioned results of the temperature-dependent semiclassical calculations with the microscopic shell model ones, also made temperature dependent. In other words, the second aim of this paper is to include temperature effects both in the microscopic shell model and (in a model-way) in the semiclassical formalism and compare the two results. It is relevant to remind here that the well known effect of adding temperature T is the washing away of the shell effects but, what may not be that well known is that the α-nucleus structure is *not* washed out [25–27]. The α-nucleus structure in nuclear interaction energy has its origin in "Wigner term" in the liquid drop energy [28,29], which is nonzero only for $N \neq Z$, non-α nuclei and gets reduced if the liquid drop energy is also made T-dependent [30,31]. There is no α-nucleus structure present in, e.g., two-center shell model [32]. It is important to realize the above-noted facts, since the microscopic spin-orbit interaction potential contains both the shell and α-nucleus structure effects, normally termed simply as the "shell effects."

The paper is organized as follows. Section II gives the methodology, consisting of the energy density formalism based on both the microscopic shell model and semiclassical approaches, with temperature effects included in both of them. Our calculations are discussed in Sec. III. We support our calculations with the data on measured mass spectrum of 75 or 80.6 MeV ($E_{\text{c.m.}} = 53.6$ or 57.6 MeV, respectively) ^{16}O+^{40}Ca $\rightarrow$ ^{56}Ni* and 88.8 MeV ($E_{\text{c.m.}} = 44.4$ MeV) ^{24}Mg+^{24}Mg $\rightarrow$ ^{48}Cr* reactions, showing explicit preference for the α-particle transfer channels [33–35]. The gradual suppression of preference for the α-particle transfer products, observed for the addition of two and four neutrons to ^{56}Ni*

channels [34], is illustrated here for adding four neutrons to ^{48}Cr*, i.e., for the compound system ^{52}Cr*. The energies involved in above reactions correspond to 1.5 to 2 times the Coulomb barrier which, e.g., lies at about 24 MeV for ^{16}O+^{40}Ca reaction. Thus, the compound nucleus temperatures involved are of the order of $\sim$3.5 MeV or more ($E^*_{\text{CN}} = E_{\text{c.m.}} + Q_{\text{in}} = (A/9)T^2 - T$). Note that the same compound system ^{56}Ni* or ^{48}Cr* is formed via the transfer products, say, the ^{28}Si+^{28}Si or ^{12}C+^{36}Ar, respectively [33,36], and hence our results could also be interpreted from the point of view of the entrance channel effects. Finally, a summary of our results is presented in Sec. IV, and Appendices A and B give the detailed solution of the spin-orbit interaction potential, respectively, for shell model and semiclassical approaches with temperature-dependence included.

II. METHODOLOGY

A. The energy density formalism (EDF)

The energy density formalism defines the interaction potential as

$$V(R) = E(R) - E(\infty), \tag{1}$$

i.e., the nucleus-nucleus interaction potential $V(R)$, as a function of relative separation distance R, is the difference of the energy expectation value E of the colliding nuclei that are overlapping (at a finite separation distance R) and are completely separated (at $R = \infty$), where

$$E = \int H(\vec{r})d\vec{r}, \tag{2}$$

with the Skyrme Hamiltonian density

$$\begin{aligned}
H(\rho, \tau, \vec{J}) = {} & \frac{\hbar^2}{2m}\tau + \frac{1}{2}t_0\left[\left(1 + \frac{1}{2}x_0\right)\rho^2 - \left(x_0 + \frac{1}{2}\right)\left(\rho_n^2 + \rho_p^2\right)\right] \\
& + \frac{1}{12}t_3\rho^{\alpha_0}\left[\left(1 + \frac{1}{2}x_3\right)\rho^2 - \left(x_3 + \frac{1}{2}\right)\left(\rho_n^2 + \rho_p^2\right)\right] \\
& + \frac{1}{4}\left[t_1\left(1 + \frac{1}{2}x_1\right) + t_2\left(1 + \frac{1}{2}x_2\right)\right]\rho\tau \\
& - \frac{1}{4}\left[t_1\left(x_1 + \frac{1}{2}\right) - t_2\left(x_2 + \frac{1}{2}\right)\right](\rho_n\tau_n + \rho_p\tau_p) \\
& + \frac{1}{16}\left[3t_1\left(1 + \frac{1}{2}x_1\right) - t_2\left(1 + \frac{1}{2}x_2\right)\right](\vec{\nabla}\rho)^2 \\
& - \frac{1}{16}\left[3t_1\left(x_1 + \frac{1}{2}\right) + t_2\left(x_2 + \frac{1}{2}\right)\right] \\
& \times \left[\left(\vec{\nabla}\rho_n\right)^2 + \left(\vec{\nabla}\rho_p\right)^2\right] \\
& - \frac{1}{2}W_0[\rho\vec{\nabla}\cdot\vec{J} + \rho_n\vec{\nabla}\cdot\vec{J}_n + \rho_p\vec{\nabla}\cdot\vec{J}_p]. \\
= {} & H(\rho, \tau) + H(\rho, \vec{J}). \tag{3}
\end{aligned}$$

Here, $\rho = \rho_n + \rho_p$, $\tau = \tau_n + \tau_p$, $\vec{J} = \vec{J}_n + \vec{J}_p$ are the nuclear, kinetic energy, and spin-orbit densities, respectively (the subscripts n and p refer to neutron and proton, respectively). m is the nucleon mass. The Coulomb effects are neglected in the above energy density functional, but can be added directly. x_0, x_1, x_2, x_3, t_0, t_1, t_2, t_3, α_0 and W_0 are the Skyrme force parameters, fitted by different authors to obtain better descriptions of various ground state properties of nuclei. In this work, we use the Skyrme forces SIII and SLy4 whose parameters are SIII: $t_0 = -1128.75$ MeV fm^3, $t_1 = 395$ MeV fm^5, $t_2 = -95$ MeV fm^5, $t_3 = 14000$ MeV fm^4, $x_0 = 0.45$, $x_1 = 0$,

$x_2 = 0$, $x_3 = 1$, $W_0 = 120$ MeV fm^5, $\alpha_0 = 1$, and SLy4: $t_0 = -2488.9$ MeV fm^3, $t_1 = 486.82$ MeV fm^5, $t_2 = -546$ MeV fm^5, $t_3 = 13777$ MeV fm^4, $x_0 = 0.834$, $x_1 = -0.344$, $x_2 = -1$, $x_3 = 1.354$, $W_0 = 123$ MeV fm^5, $\alpha_0 = 0.167$, respectively. Thus, for spin-orbit density part of the interaction potential, both the cases of $x_2 = 0$ and -1 are studied [see below and in Appendix B for the role of parameter x_2 in effective mass parameter $f_q(\vec{r})$], which refer to very old and rather new Skyrme forces, respectively.

Since we are interested here only in spin-orbit density part of the interaction potential, we neglect the spin-independent part of the Hamiltonian density $H(\rho, \tau)$ in Eq. (3), and write

$$V_J(R) = \int \{H(\rho, \vec{J}) - [H_1(\rho_1, \vec{J}_1) + H_2(\rho_2, \vec{J}_2)]\}d\vec{r} \quad (4)$$

with $\rho = \rho_1 + \rho_2$ and $\vec{J} = \vec{J}_1 + \vec{J}_2$ for the composite system, in sudden approximation [37]. We use the sudden approximation because it is only in this approximation that the different terms of $H(\rho, \vec{J})$ in Eq. (4) are shown to constitute the nuclear proximity potential [38] used here (Appendix B), like for the spin-independent part $H(\rho, \tau)$ in Refs. [39,40]. The other alternative is to use the adiabatic approximation, but then $V_J(R)$ could not be defined by Eq. (4) since the collisions, being then slow, allows the system to adjust itself to an equilibrium configuration at each stage (r-value) of the collision. In the following, we solve this equation in two different ways, i.e., by using the microscopic shell model and the semiclassical ETF approaches, which are made temperature dependent since the composite or compound systems formed are hot.

1. The microscopic approach

Defining n_i as the occupation probability of the ith single-particle state ϕ_i, which depends on temperature T (in MeV), we can write [41]

$$\rho_q(\vec{r}) = \sum_{i,s} n_i |\phi_i(\vec{r}, s, q)|^2, \quad (5)$$

$$\vec{J}_q(\vec{r}) = (-i) \sum_{i,s,s'} n_i \phi_i^* [\vec{\nabla}\phi_i(\vec{r}, s', q) \times \langle s|\sigma|s'\rangle] \quad (6)$$

with

$$N = \sum_i n_i = \sum_i \left[1 + \exp\frac{(\varepsilon_i - \lambda)}{T}\right]^{-1}. \quad (7)$$

Apparently, $n_i = 1$ for $T = 0$; and N is the number of particles since the summation i is over all the occupied single particle states of energies ε_i. s and $q(=n$ or $p)$ represent the spin and isospin indices, respectively, and λ is the Fermi surface, determined by requiring the total number of particles N to be conserved. The single particle energies ε_i are calculated by using the standard shell model Hamiltonian, and the spherically symmetric single particle wave functions are taken to be as follows for both the closed and un-closed shell

nuclei [1,11]:

$$\phi_i(\vec{r}, s, q) = \frac{R_\alpha(r)}{r} \sum_{m_\ell m_s} \left\langle \ell\frac{1}{2}m_\ell m_s \middle| jm \right\rangle Y_\ell^{m_\ell}(\hat{r})\chi_{m_s}(s)\chi_q(t), \quad (8)$$

where $\alpha = (q, i) \equiv (q, n, \ell)$. For use of Eq. (8), Eqs. (5) and (6) simplify as

$$\rho_q(r) = \frac{1}{4\pi r^2} \sum_\alpha n_\alpha(2j_\alpha + 1)R_\alpha^2(r), \quad (9)$$

$$\vec{J}_q(\vec{r}) = \frac{\vec{r}}{4\pi r^4} \sum_\alpha n_\alpha(2j_\alpha + 1)$$
$$\times \left[j_\alpha(j_\alpha + 1) - \ell_\alpha(\ell_\alpha + 1) - \frac{3}{4}\right] R_\alpha^2(r). \quad (10)$$

The normalized radial wave functions $R_\alpha(r)$ of the shell model of the nucleus are given as [1]

$$R_\alpha(r) = C_\alpha r^{l+1} e^{-\nu r^2} \upsilon_\alpha(2\nu r^2) \quad (11)$$

with

$$C_\alpha = \left[\frac{2^{l-n+2}(2\nu)^{l+3/2}(2l + 2n + 1)!!}{\sqrt{\pi}[(2l + 1)!!]^2 n!}\right]^{1/2}, \quad (12)$$

$$\upsilon_\alpha(x) = \sum_{k=0}^{n}(-1)^k 2^k ({}^nC_k)\frac{(2l + 1)!!}{(2l + 2k + 1)!!}x^k \quad (13)$$

and

$$2\nu = \frac{41A^{-1/3}mc^2}{\hbar^2 c^2} \quad \text{(in fm}^{-2}). \quad (14)$$

Using Eqs. (9) and (10) in Eq. (4), we get the spin-orbit density part of the interaction potential $V_J(R)$, whose details of solution for $\rho_n = \rho_p = \frac{1}{2}\rho_i$ are given in Appendix A. Note that for $T = 0$ ($n_\alpha = 1$), $\vec{J} = 0$, and hence the $V_J(R)$ will be zero if the nucleus is with a major shell closed, i.e., the orbits with $j = l \pm \frac{1}{2}$ pair are fully occupied. However, for $T \neq 0$, $n_\alpha < 1$ and hence $\vec{J} \neq 0$ always (closed or unclosed shell nuclei).

2. The semiclassical approach

The spin, being a purely quantal property, has no classical analogue, which means there is no contribution to the semi-classical functional of $\vec{J}$ in the lowest order at the so-called Thomas-Fermi (TF) level. However, at the ETF level one obtains the higher order contributions [16–18], and as the second order contribution is enough for numerical convergence [18], we have for the semiclassical spin-orbit density ($q = n$ or p; $i = 1,2$)

$$\vec{J}_q(\vec{r}) = -\frac{2m}{\hbar^2}\frac{1}{2}W_0\frac{1}{f_q}\rho_q\vec{\nabla}(\rho_i + \rho_q) \quad (15)$$

with f_q as the effective mass form factor,

$$f_q(\vec{r}) = \frac{m}{m_q^*(\vec{r})}$$

$$= 1 + \frac{2m}{\hbar^2}\left[\frac{1}{4}\left\{t_1\left(1+\frac{x_1}{2}\right)+t_2\left(1+\frac{x_2}{2}\right)\right\}\rho_i(\vec{r})\right.$$

$$\left.-\frac{1}{4}\left\{t_1\left(x_1+\frac{1}{2}\right)-t_2\left(x_2+\frac{1}{2}\right)\right\}\rho_q(\vec{r})\right]. \quad (16)$$

For nuclear density ρ_i, we use the two parameter Fermi density distribution, which is made T-dependent as [23]

$$\rho_i(r) = \rho_{0i}(T)\left[1+\exp\frac{r-R_{0i}(T)}{a_i(T)}\right]^{-1}, \quad (17)$$

with central density

$$\rho_{0i}(T) = \frac{3A_i}{4\pi R_{0i}^3(T)}\left[1+\frac{\pi^2 a_i^2(T)}{R_{0i}^2(T)}\right]^{-1} \quad (18)$$

and half density radii $R_{0i}(T=0)$ and the surface thickness parameters $a_i(T=0)$ obtained by fitting the experimental data [42,43] to the polynomials in nuclear mass $A (= 4$–$209)$, as (see Fig. 1)

$$R_{0i}(T=0) = 0.90106 + 0.10957A_i - 0.0013A_i^2 + 7.71458$$
$$\times 10^{-6}A_i^3 - 1.62164 \times 10^{-8}A_i^4, \quad (19)$$

$$a_i(T=0) = 0.34175 + 0.01234A_i - 2.1864 \times 10^{-4}A_i^2$$
$$+ 1.46388 \times 10^{-6}A_i^3 - 3.24263 \times 10^{-9}A_i^4. \quad (20)$$

It is for the first time that such a data is used in calculations based on semiclassical approach. In all earlier calculations [18, 20,21], these parameters were determined self-consistently. All of these calculations (the HF, the ETF, and the SM) give similar densities, and are comparable with Fermi density at $T = 0$, atleast in the tail/surface region of interest for heavy ion collisions. This is illustrated in Fig. 2 for two nuclei (one light and other heavy) where HF and ETF density calculations are
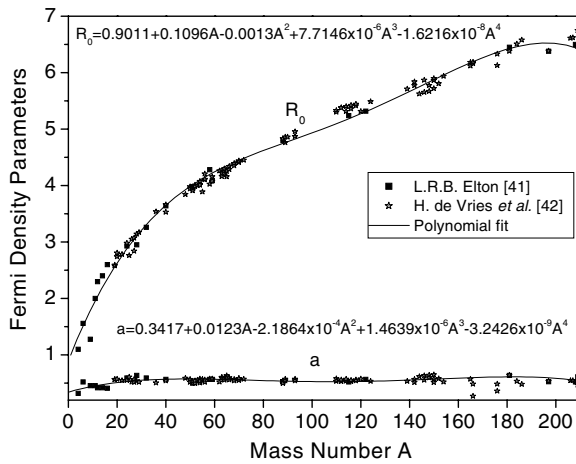

FIG. 1. The half-density radius R_0 and the surface thickness a in fm, plotted as a function of mass number A of nuclei, each fitted to a polynomial in A. The data are from [42,43].
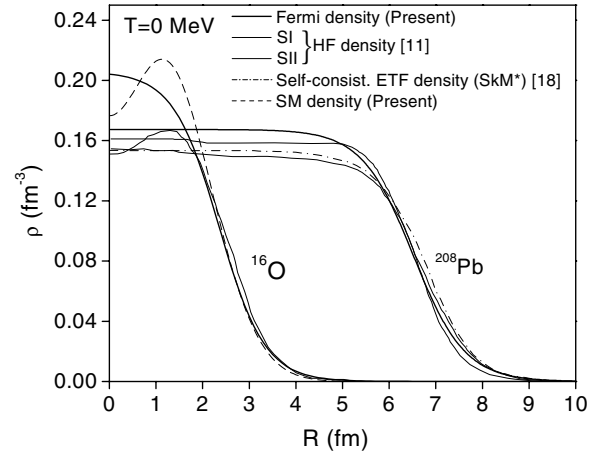

FIG. 2. The Fermi density compared with HF, ETF, and SM density distributions at $T = 0$ for ^{208}Pb and ^{16}O nuclei. The HF and ETF calculations are from [11] and [18], respectively.

available in the literature [11,18]. For ^{208}Pb, the Fermi density (17) is compared with the HF density, calculated for two different Skyrme forces SI and SII [11], and the ETF density for Skyrme SkM* force [18]; and for ^{16}O with HF density for Skyrme SI force and the shell model (SM) density (9). Since nuclear densities are the main input in the semiclassical ETF model, apparently, our use of the SM wave functions, instead of the HF equations, and the Fermi density, instead of the self-consistent HF/ETF densities, are quite reasonable.

The temperature dependence in the above formulas is introduced as in Ref. [44],

$$R_{0i}(T) = R_{0i}(T=0)[1+0.0005T^2] \quad (21)$$

and

$$a_i(T) = a_i(T=0)[1+0.01T^2]. \quad (22)$$

The spin-orbit interaction potential $V_J(R)$ is then obtained by solving Eq. (4) for $\rho_n = \rho_p = \frac{1}{2}\rho_i$; $i = 1, 2$, expressed as the proximity potential [38]. The details of this method are summarized in Appendix B.

III. CALCULATIONS AND DISCUSSION OF RESULTS

In this section, we discuss our calculations of the spin-orbit interaction potentials for two nucleon transfer products in the reactions ^{28}Si+^{28}Si and ^{24,26}Mg+^{24,26}Mg forming the compound systems ^{56}Ni* and ^{48,52}Cr*, using both the semiclassical and microscopic approaches and for two Skyrme forces SIII and SLy4. Since, by definition, the formation of compound system is independent of the entrance channel effects, the ^{56}Ni* and ^{48}Cr*, say, could also be considered to be formed from any two other nuclei, such as ^{16}O+^{40}Ca and ^{16}O+^{32}S, respectively. The important point is that during the transfer process, the spin-unsaturated ($\vec{J}_i \neq 0$) reaction partners would become with either one or both spin-saturated nuclei, and vice-versa. In the following, we first consider the case of temperature $T = 0$ and then include the temperature effects in the calculation of spin-orbit interaction potential.
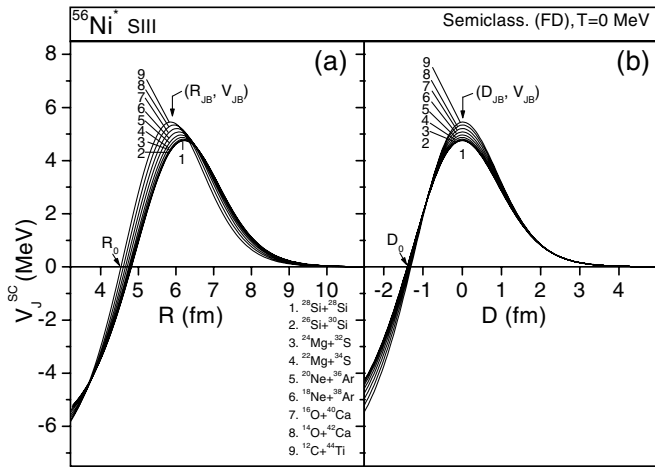
FIG. 3. (a) The spin-orbit interaction potential $V_J^{SC}(R)$, and (b) $V_J^{SC}(D)$, for two nucleon transfer products, starting from ^{28}Si+^{28}Si, using the semiclassical approach for Skyrme force SIII.

A. Spin-orbit interaction potentials at temperature $T = 0$

Figure 3(a) shows the spin-orbit interaction potential $V_J^{SC}(R)$, calculated by using the semiclassical approach with Skyrme force SIII, for two nucleon transfer products starting with the target-projectile combination ^{28}Si+^{28}Si. Note that the spin-orbit interaction potential is independent of the charge of colliding nuclei and hence the transfer of two neutrons or two protons leads to the same result. Comparing this figure with Fig. 4(a), showing the results of the same calculation for use of the microscopic shell model approach, we notice the following points of differences:

(i) Whereas in the semiclassical approach the barrier height V_{JB}^{SC} increases continuously [see Fig. 5(a)], the same in microscopic shell model decreases till it becomes zero for spin-saturated nuclei and then increases as the product mass increases or decreases [see Fig. 5(b), solid line for V_{JB}^{SM}]. Almost the same

result was obtained for shell model calculations with Fermi density distribution [1,9].

(ii) In other words, in contrast to the shell model calculations, the $V_J(R)$ in semiclassical approach does not become zero for spin-saturated nuclei.

(iii) Though the maximum height of the barrier V_{JB} in two approaches is nearly of the same order, the relative increament with respect to two nucleon transfer in the semiclassical case is much smaller than in the shell model.

(iv) The position R_{JB} of the barrier in Fig. 3(a) changes and shifts to smaller R-value as the asymmetry of transfer products increases, though is placed exactly at the touching radius, i.e., $R_{JB} = R_{01} + R_{02}$ for the semi-classical approach, but it remains almost independent of the transfer process for microscopic shell model in Fig. 4(a). This result, however, becomes more evident if, in the case of semiclassical calculations, we remove the $R_{01} + R_{02}$ dependence of Fig. 3(a) by plotting instead the $V_J^{SC}(D)$, where $D = R - R_{01} - R_{02}$ is the surface separation between two nuclei. This is done in Fig. 3(b). Now the barrier position D_{JB} ($= R_{JB} - R_{01} - R_{02}$) is also independent of the transfer process and occurs at a fixed (zero) value. Note that the quantity D is of more relevance for the proximity force theorem (see Appendix B). Similarly, the sign of the potential for shell model approach changes at about the radius of the compound nucleus R_0, and that for semiclassical approach at D_0-value (equivalently, $R_0 = D_0 + R_{01} + R_{02}$). Apparently, the same result would appear on normalizing the potentials of Fig. 3(b) with respect to the potential for spin-saturated pair of nuclei (see below for normalization), i.e., all the curves would pass through nearly the same D_0-value and placed at the same $D_{JB} = 0$ (see Fig. 4(b)).

Notwithstanding the above discrepencies with microscipic shell model, the semiclassical approach is considered as well accepted, possibly because it is supposed to contain *no* shell effects or, in other words, is a liquid drop model type of
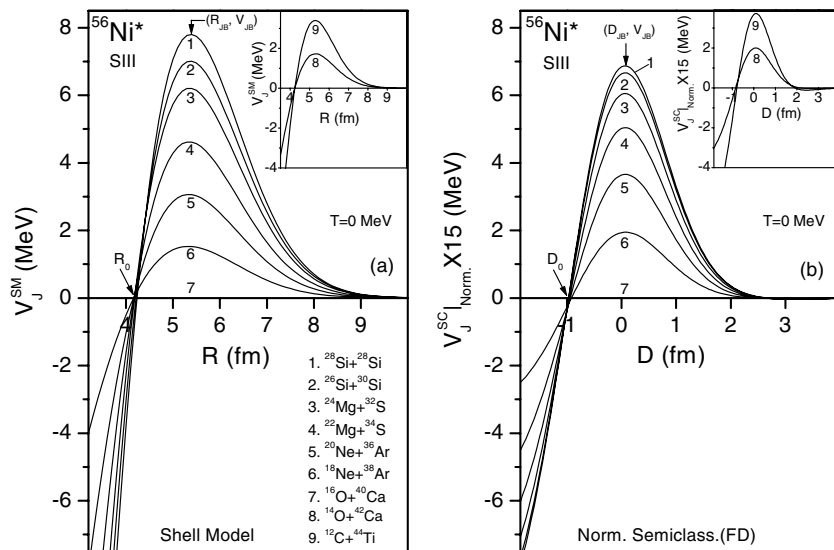

FIG. 4. (a) Same as for Fig. 3(a), but for the microscopic shell model approach. (b) Same as Fig. 3(b), but now the normalized values, i.e., the $V_J^{SC}|_{Norm.}(D)$ with respect to curve 7 in part (a). The plotted values are 15 times more than the ones obtained on normalization.
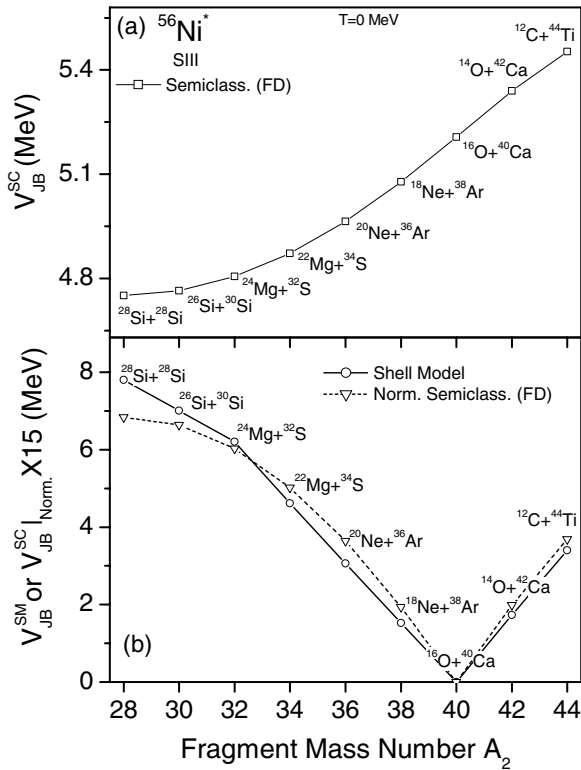
FIG. 5. (a) Spin-orbit interaction barriers V_{JB}^{SC} as a function of the mass numbers of the heavier transfer products in the reaction $^{28}Si+^{28}Si$ forming $^{56}Ni^*$, using the semiclassical approach with Skyrme force SIII. (b) The same as in (a) but for the microscopic shell model approach, i.e., V_{JB}^{SM}, and from the semiclassical calculations after their normalization to zero for spin-saturated combination $^{16}O+^{40}Ca$, i.e., $V_{JB}^{SC}|_{Norm.} \times 15$.

description [18]. In the following, however, we show that the semiclassical approach can reproduce the same effects as are present in microscopic shell model if the results of semiclassical calculations are normalized with respect to its result for spin-saturated nuclei. The origin of such an arbitrary normalization factor in semiclassical theory, however, still remains to be traced.

Realising that the spin-orbit interaction $V_J(R)$ for a spin-saturated pair of nuclei ($^{16}O+^{40}Ca$ for compound system $^{56}Ni^*$, i.e., curve 7 in Fig. 3) should be zero, we have normalized all the curves in Fig. 3(b) to curve 7 to be zero, by defining the normalized semiclassical spin-orbit interaction potentials $V_{JB}^{SC}|_{Norm.}$ at each D as follows:

$$V_J^{SC}|_{Norm.}(D) = \mp \left[V_J^{SC}(D) - V_{J,SS}^{SC}(D) \right], \quad (23)$$

where $V_{J,SS}^{SC}$ refers to the V_J^{SC} for the closed-shell, spin-saturated pair of nuclei in Fig. 3(b) (curve 7), and the (arbitrarily added) sign ($-$) or ($+$) to the combinations before and after the spin-saturated pair of nuclei. Apparently, this kind of normalization is applicable to regions of nuclei where magic shells are well established, which means to exculde at present the exotic nuclei far from the valley of stability and the superheavy nuclei. The above normalization (with sign change to be added later) follows from the definition of normalized

semiclassical spin-orbit density of a nucleus:

$$\vec{J}_i^{SC}|_{Norm.}(\vec{r}) = \left[\vec{J}_i^{SC}(\vec{r}) - \vec{J}_{i,SS}^{SC}(\vec{r}) \right], \quad (24)$$

where the $\vec{J}_i^{SC}(\vec{r})$ ($i=1,2$) refers to the semiclassical spin-orbit density in Eq. (B1). Then, the $V_J^{SC}|_{Norm.}(D)$ from Eq. (23) is plotted in Fig. 4(b) by introducing a multiplication factor A to match the shell model amplitude for V_{JB}^{SM} at $R = R_{JB}$, i.e.,

$$V_{JB}^{SM}(R_{JB}) \equiv A \times V_{JB}^{SC}|_{Norm.}(D_{JB}). \quad (25)$$

We find that, for the system under study, with a factor of $A = 15$ the normalized semiclassical spin-orbit potentials $V_J^{SC}|_{Norm.}(D)$ in Fig. 4(b) reproduce completely the structure of shell model calculations in Fig. 4(a). The factor of 15 is though arbitrary, but constant for all transfer products. In other words, though the normalized semiclassical spin-orbit interaction potentials are too small by a factor of 15, they contain exactly the same shell structure effects as are present in microscopic shell model calculations. This is further stressed in Fig. 5(b) where the spin-orbit barrier heights V_{JB}^{SM} for shell model are compared with $V_{JB}^{SC}|_{Norm.}$ of the normalized semiclassical calculations. Apparently, we get the one-to-one correspondence for the magnitudes, though there is a significant difference in the structure of the two curves [solid for $V_{JB}^{SM}(A_2)$ and dashed for $V_{JB}^{SC}|_{Norm.}(A_2)$], which refers to the α-nucleus structure, to be discussed below. The above results are independent of the choice of Skyrme force, as well as of the compound system. This is illustrated in Fig. 6 for $^{56}Ni^*$ using SLy4, and in Fig. 7 for $^{48,52}Cr^*$ using SIII parameter set, only for the barrier positions. The factor of 15 remains the same for SLy4 force and for $^{52}Cr^*$ system, but reduces to 11
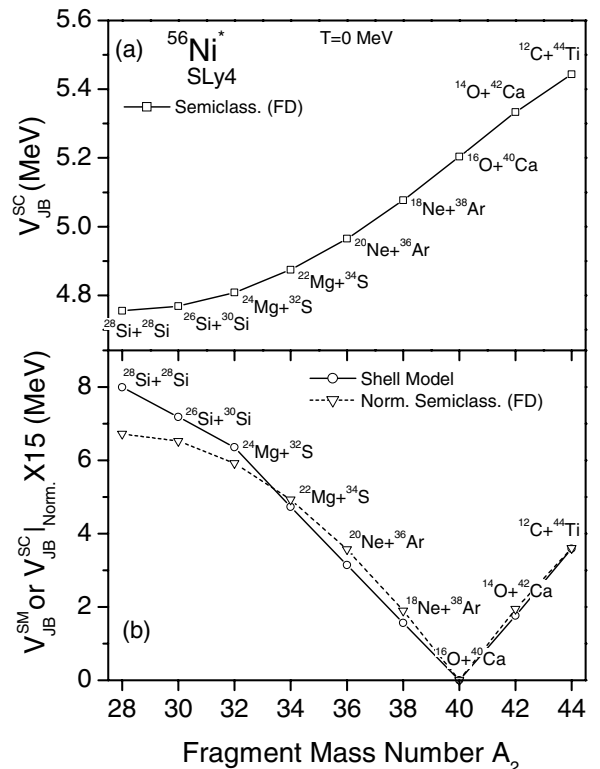

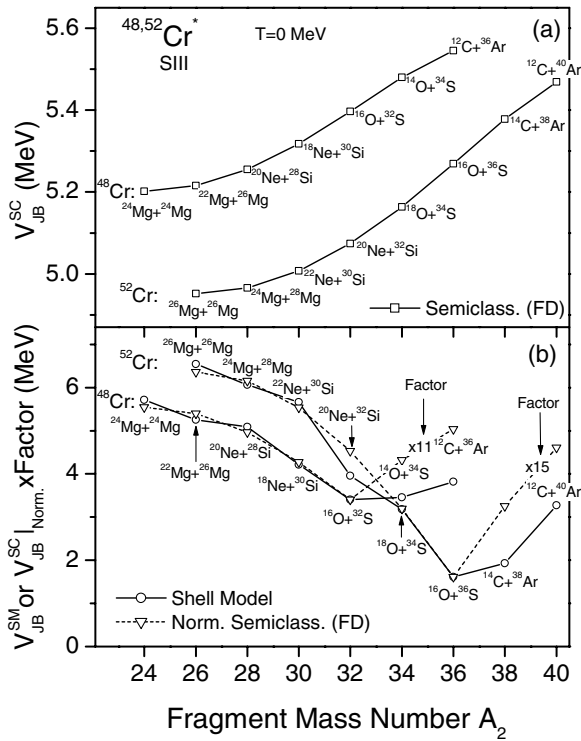
FIG. 6. Same as for Fig. 5, but for the Skyrme force SLy4.

FIG. 7. Same as for Fig. 5, but for ^{24,26}Mg+^{24,26}Mg reactions forming ^{48,52}Cr*.

FIG. 8. The Fermi density and microscopic shell model density distributions at temperaturs $T = 0$ and 5.0 MeV.

for the lighter compound system ^{48}Cr*. The small discrepency in the first two points of Figs. 5(b) and 6(b) and last two points of Fig. 7(b) calls for different multiplying factors. Note that in ^{48,52}Cr*, only one of the reaction partners is a spin-saturated nucleus (^{16}O in ^{16}O+^{32}S and ^{16}O+^{36}S), and hence we have normalized the semiclassical calculations to the microscopic shell model results, instead of to zero.

Looking at $N = Z$, $A = 4n\,\alpha$ multiplier compound systems in Figs. 5(b), 6(b), and 7(b) more closely, we notice that the shell model calculations (solid lines) present a preference for α nucleus transfer products in terms of a discontinuity (or step) in the barriers at the α-nucleus transfer products. This effect is shown [9] related to the closure of last j shell for *both* the protons and neutrons of atleast one of the product nucleus, as is the case here. However, such a preference is not shown in Fig. 7(b) (solid line for V_{JB}^{SM}) for the non-α multiplier compound system ^{52}Cr*, in agreement with experiments [34]. This problem is discussed in detail in the earlier work of one of us (R.K.G.) and Collaborators [9]. On the other hand, the above noted discontinuity at α-nucleus transfer products in $N = Z\,\alpha$-nucleus systems seems missing in the normalized semiclassical calculations [dashed lines in Figs. 5(b), 6(b) and 7(b)], which, when combined with the results of the last paragraph, can be interpreted to mean that, in the normalized semiclassical approach, the α-nucleus structure seems absent though it still seems to contain the shell structure like effects. Here, it may be reminded again that the α-nucleus structure in nuclear interaction energy is related to the "Wigner term" in the liquid drop energy (which is zero for $N = Z$, α-nuclei) [30] and that there is no α-nucleus structure present in shell model of the nucleus [32].
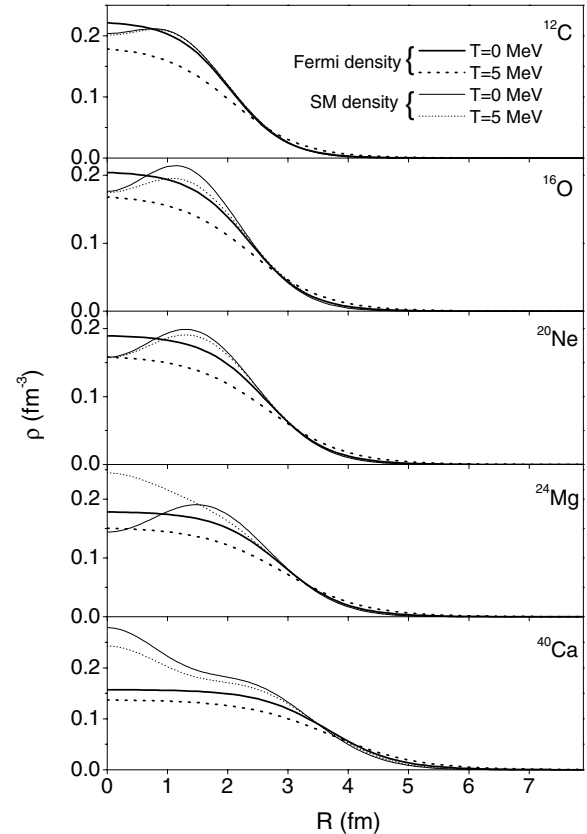
B. Spin-orbit interaction potentials at finite temperatures

First of all, in Fig. 8, we compare the Fermi density and microscopic shell model density distributions at two temperatures for a few illustrative nuclei involved in the above chosen transfer reactions. We notice that in the surface region, relevant for heavy ion collisions, the two distributions match not only for temperature $T = 0$, but also for a very high $T = 5$ MeV. This means to suggest that our model prescription for the T-dependence of Fermi density used in semiclassical approach is reasonbly good, as compared to the microscopic T-dependence of shell model density.

Figures 9 and 10 show, respectively, the semiclassical and microscopic shell model spin-orbit interaction potentials at different temperatures, ranging from 0 to 5 MeV, for the compound system ^{56}Ni* using Skyrme force SIII. We notice that in both cases, as expected, the barriers decrease with increase of temperature, but still there is an important point of difference in the T-dependence of the two approaches: Whereas the order (1 to 9) of barriers remains the same in semiclassical case, the same in microscopic shell model approach changes due to the different filling of shell model states (occupation number n_α decreases with T, with particle number N conserved). Thus, it again seem as if there were no shell-like effects in semiclassical approach. However, if we compare in Fig. 11 the normalized spin-orbit interaction barriers $V_{JB}^{SC(T)}|_{Norm.}(A_2)$ of semiclassical approach with $V_{JB}^{SM(T)}(A_2)$ of the shell model,

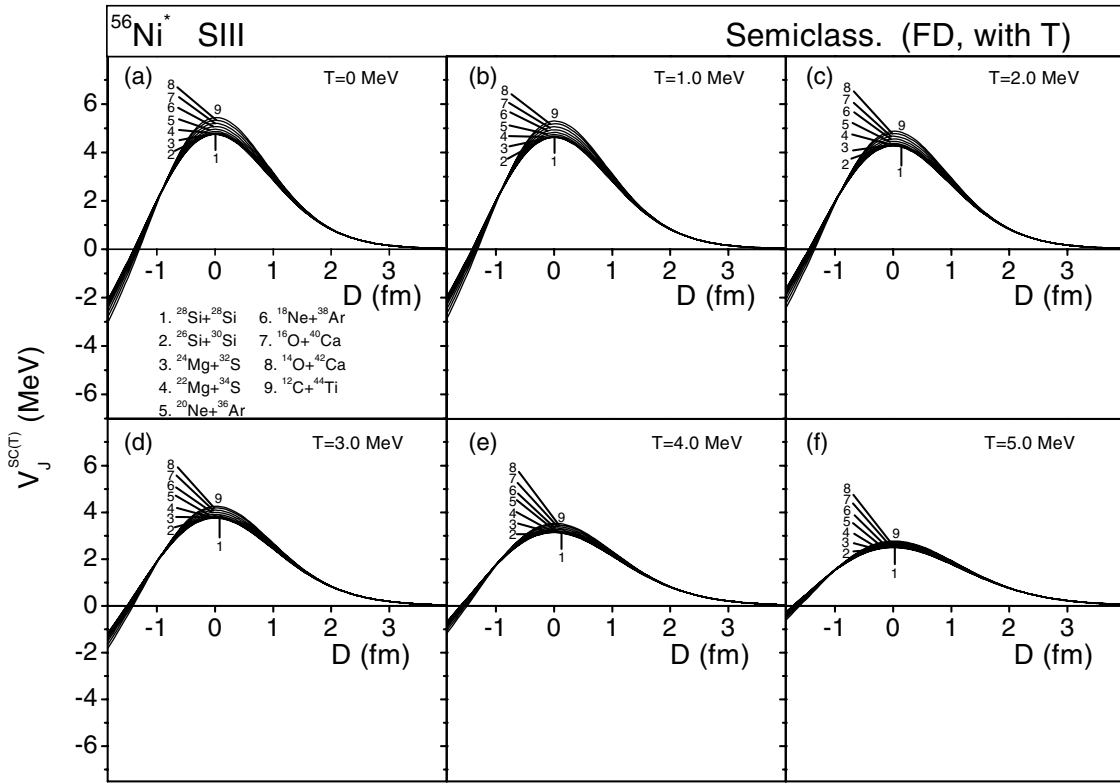FIG. 9. The spin-orbit interaction potentials for different transfer products of the reaction ^{28}Si+^{28}Si forming ^{56}Ni* at different temperatures ranging from 0 to 5 MeV for Skyrme force SIII, using the T-dependent semiclassical approach.
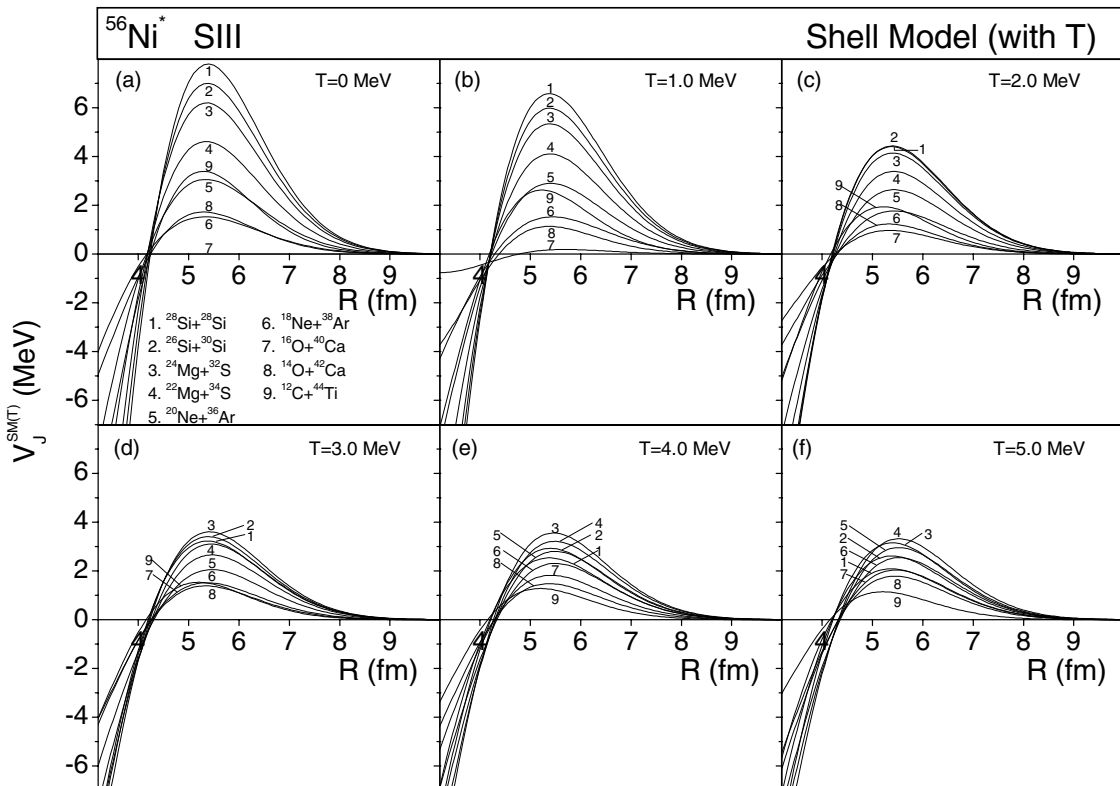

FIG. 10. Same as for Fig. 9, but for the T-dependent microscopic shell model approach.
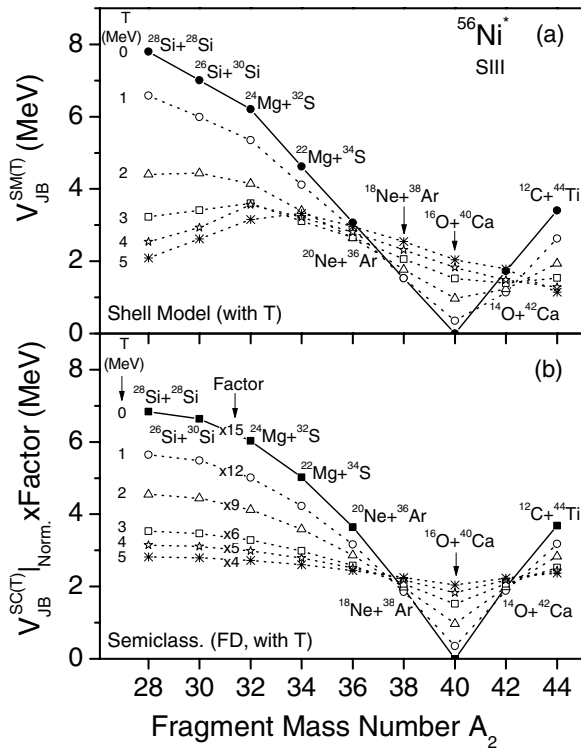
FIG. 11. The spin-orbit interaction barriers, plotted as a function of the mass number of one of the transfer products for different temperatures, calculated on the T-dependent microscopic shell model approach and compared with normalized spin-orbit interaction barriers calculated on the T-dependent semiclassical approach, using SIII force parameters for the compound system ^{56}Ni*. The normalization of the semiclassical results to the shell model results is carried at each temperature for the spin-saturated combination ^{16}O+^{40}Ca.

we find an almost one-to-one correspondence provided the multiplying factor is also made T-dependent. Figure 11 shows our calculation for the compound system ^{56}Ni* using SIII force. The same results are obtained for the SLy4 force and the compound systems ^{48,52}Cr* (not shown here). The comparisons are very good for temperatures up to $T = 3$ MeV, but for the higher temperatures a single multiplying factor seems to be not enough for both the symmetric and asymmetric fragments.

Furthermore, we notice in Fig. 11 that the α nucleus structure remains unaffected with temperature. In other words, the α nucleus structure in shell model barriers remains apparent at all temperatures, but the same is absent at all temperatures in the (normalized) semiclassical interaction barriers. Another interesting result that follows from this figure is the increase or decrease of the barriers with temperature due to the shell structure of nuclei, i.e., with respect to the major shell closed nuclei (for both neutrons and protons, or only for neutrons or protons), closed j shell nuclei or the unclosed shell nuclei. This is explicilty demonstrated in Fig. 12. In this figure we notice that the barriers increase with temperature for major closed shell nuclei such as ^{16}O+^{40}Ca and its neighboring combinations ^{14}O+^{42}Ca and ^{18}Ne+^{38}Ar, decrease for j shell closed nuclei like ^{28}Si+^{28}Si, ^{26}Si+^{30}Si, ^{24}Mg+^{32}S, and ^{12}C+^{44}Ti, and remain nearly unaffected for
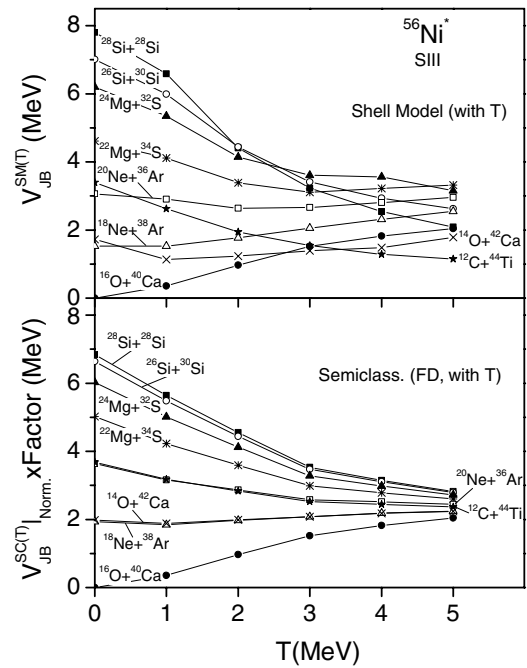

FIG. 12. The same as for Fig. 11, but plotted as a function of temperature T, and for different transfer products.

unclosed shell nuclei like ^{20}Ne+^{36}Ar and ^{22}Mg+^{34}S. This change is more pronounced for $T = 0$ to 3 MeV since the shell effects are known to get reduced to almost zero at about 3 MeV.

IV. SUMMARY

In this paper, we have attempted for the first time to compare the semiclassical formulation of the Skyrme energy density functional with the microscopic shell model formulation, in particular for the spin-orbit density part of the interaction potential. This is done for both the ground state (temperature $T = 0$) and for finite temperatures of the hot compound nucleus. The semiclassical approach, in extended Thomas-Fermi (ETF) model, is used up to its second order terms of spin-orbit density, with nuclear density taken as the two parameter Fermi density whose half-density radius and surface thickness parameters, obtained by fitting the available experimental data, are made temperature dependent. The temperature dependence in microscopic shell model is introduced via the Fermi-Dirac occupation of states and particle number conservation. Our calculations are made for three two-nucleon transfer reactions forming both the α-multiplier $A = 4n$, $N = Z$ and non-α-multiplier $A \neq 4n$, $N \neq Z$ compound systems, and for Skyrme forces SIII and SLy4.

We find that, against the general belief, (normalized) semiclassical spin-orbit interaction potential does contain exactly the same shell-like effects as are present in microscopic shell model. It is true that the semiclassical spin-orbit interaction potential is not zero for spin-saturated nuclei, but if the interaction potentials for spin-unsaturated nuclei are normalized to the interaction potential of spin-saturated pair (for one or

both the nuclei as spin-saturated), which in turn is also made zero, then the normal shell effects are obtained in semiclassical spin-orbit interaction potential. What may be missing in the semiclassical approach is the α nucleus structure, seen in microscopic shell model for α nucleus transfer product(s) with its last j shell completely filled for both protons and neutrons. This result is found to be independent of both the mass of compound system and the choice of Skyrme force parameter. Note that the α nucleus structure is related to the Wigner term in liquid drop energy, and not to the shell model of the nucleus.

Finally, our model prescription of the T-dependence of Fermi density is found nearly identical to the microscopic T-dependence of the shell model density. Its role is shown in increasing or decreasing the height of the (normalized) barrier as per the shell structure of the transfer products, and show almost no change in the behavior of shell and α nucleus structure effects in both the (normalized) semiclassical and microscopic shell model spin-obit interaction potentials, at least up to 3 MeV. The barriers are found to increase with temperature for major closed shell nuclei, decrease for j shell closed nuclei, but remain nearly unchanged for unclosed shell nuclei.

APPENDIX A: SOLUTION OF THE SPIN-ORBIT INTERACTION POTENTIAL USING THE MICROSCOPIC APPROACH

In the approximation of equal neutrons and protons densities ($\rho_n = \rho_p = \frac{1}{2}\rho_i$; i=1,2), Eqs. (3) and (4) give the spin-orbit density dependent part of the interaction potential

$$V_J(R) = -\frac{3}{4}W_0 \int \{\rho_2 \vec{\nabla} \cdot \vec{J}_1 + \rho_1 \vec{\nabla} \cdot \vec{J}_2\} d\vec{r}$$
$$= V_{J_1}(R) + V_{J_2}(R). \quad \text{(A1)}$$

Notice here that we need to solve only one of the terms, since one term can be obtained from the other by simply interchanging 1 and 2.

Using Eq. (11) in Eq. (9), the microscopic shell model density for a nucleus (neutrons+protons) can be expressed simply as ($i = 1,2$)

$$\rho_i(r_i) = \rho_{0i}\left(a_0 + a_1 y_i + a_2 y_i^2 + \cdots\right)\exp\left(-y_i\right) \quad \text{(A2)}$$

with $y_i = 2\nu_i r_i^2$, the central density $\rho_{0i} = 4\pi^{-3/2}(2\nu_i)^{3/2}$, and $a_0(=1), a_1, a_2, \ldots$ as the constants. Also, it follows from Fig. 13, that

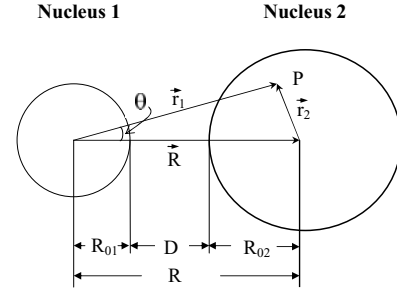$$r_2^2 = r_1^2 + R^2 - 2r_1 R \cos\theta \qquad 0 \leqslant r \leqslant \infty. \quad \text{(A3)}$$

FIG. 13. Geometry of two colliding spherical nuclei.

Next, noting that $\vec{J}_q$ depends only on $\vec{r}$, using Eq. (10) in the following known divergence relation:

$$\vec{\nabla} \cdot \vec{A} = \frac{1}{r^2}\frac{\partial}{\partial r}(r^2 A_r), \quad \text{(A4)}$$

we get for a nucleus ($\vec{J}_1 = \vec{J}_n + \vec{J}_p$),

$$\vec{\nabla} \cdot \vec{J}_1 = \sum_\alpha \left[\frac{P_\alpha}{r_1^2}U_\alpha^2(r_1) + \frac{2P_\alpha}{r_1}U_\alpha(r_1)\frac{\partial}{\partial r_1}U_\alpha(r_1)\right], \quad \text{(A5)}$$

where we have denoted $U_\alpha(r) = R_\alpha(r)/r$ and

$$P_\alpha = \frac{n_\alpha}{4\pi}(2j_\alpha + 1)\left[j_\alpha(j_\alpha + 1) - \ell_\alpha(\ell_\alpha + 1) - \frac{3}{4}\right].$$

This equation (A5), together with Eq. (A2), on substitution in Eq. (A1), gives (for $\mu = \cos\theta$)

$$V_{J_1}(R) = -\frac{3\pi}{2}W_0 \int_0^\infty I(y_2)$$
$$\times \sum_\alpha \left[\frac{P_\alpha}{r_1^2}U_\alpha^2 + \frac{2P_\alpha}{r_1}U_\alpha\frac{\partial U_\alpha}{\partial r_1}\right]r_1^2 dr_1, \quad \text{(A6)}$$

where, using $r_2^2 = r_1^2 + R^2 - 2r_1 R\mu = y_2/2\nu_2$ or $d\mu = -dy_2/4\nu_2 r_1 R$,

$$I(y_2) = \frac{\rho_{02}}{4\nu_2 r_1 R}\int_{2\nu_2(r_1-R)^2}^{2\nu_2(r_1+R)^2}\left[a_0 + a_1 y_2 + a_2 y_2^2 + \cdots\right]$$
$$\times \exp(-y_2)dy_2. \quad \text{(A7)}$$

Solving the integral $I(y_2)$ by parts, the integral (A6) is solved numerically.

APPENDIX B: SOLUTION OF THE SPIN-ORBIT INTERACTION POTENTIAL USING THE SEMICLASSICAL APPROACH

The nucleon spin-orbit density $\vec{J}_q$ ($q = n$ or p) [Eq. (15)] of the semiclassical approach, in the approximation of $\rho_n = \rho_p = \frac{1}{2}\rho_i$; i=1,2, gives the spin-orbit density of a nucleus $\vec{J}_i$ ($=\vec{J}_n + \vec{J}_p$) as

$$\vec{J}_i(\vec{r}) = -\frac{2m}{\hbar^2}\frac{3}{4}W_0\frac{1}{f_q}\rho_i\vec{\nabla}\rho_i \quad \text{(B1)}$$

with

$$f_q(\vec{r}) = 1 + \frac{2m}{\hbar^2}\left(\frac{3t_1 + 5t_2}{16} + \frac{t_2 x_2}{4}\right)\rho_i(\vec{r}). \quad \text{(B2)}$$

Then, the spin-orbit density dependent part of the Hamiltonian density [from Eq. (3)] becomes

$$H_{J_i}(\rho_i) = -\frac{2m}{\hbar^2}\left(\frac{3}{4}W_0\right)^2 \frac{1}{f_q}\rho_i(\vec{\nabla}\rho_i)^2. \qquad \text{(B3)}$$

Note that H_J is now a functional of ρ alone (f_q is also a function of ρ), independent of the shell structure of the nucleus. Observing this fact, Singh and Gupta [38] determined the spin-orbit interaction potential $V_J(R)$ [Eq. (4)] directly in terms of the proximity potential, as discussed below.

Based on Ref. [45], and following Chattopadhyay and Gupta [40], the proximity potential between two spherical nuclei of radii R_{01} and R_{02}, whose centers are separated by $R = R_{01} + R_{02} + D$, is defined by

$$V_J(R) = 2\pi \bar{R}\int_s^{\infty} e(D)dD = 2\pi\bar{R}\phi_J(D), \qquad \text{(B4)}$$

where $\bar{R} = R_{01}R_{02}/(R_{01}+R_{02})$, the mean curvature radius defining the geometry of the system, and $e(D)$ is the interaction energy per unit area between two flat parallel slabs of semi-infinite nuclear matter, with surfaces parallel to the X-Y plane, moving in the Z-direction and separated by a distance D having the minimum value s. Since the $\int e(D)dD$ is independent of the geometry, it is a universal function, given by

$$\phi_J(D) = \int\left\{H_J(\rho) - \left[H_{J_1}(\rho_1) + H_{J_2}(\rho_2)\right]\right\}dZ. \qquad \text{(B5)}$$

For the slab approximation, the two parameter Fermi density becomes ($i = 1,2$)

$$\rho_i(Z_i) = \rho_{0i}(T)\left[1 + \exp\frac{Z_i - R_{0i}(T)}{a_i(T)}\right]^{-1} \quad -\infty \leqslant Z \leqslant \infty \qquad \text{(B6)}$$

with

$$Z_2 = R - Z_1.$$

Substituting Eq. (B6) in Eq. (B3), we get from Eq. (B5) the universal function $\phi_J(D)$, solved numerically for the spin-orbit interaction potential $V_J(R)$ in Eq. (B4). For more details, see Ref. [38].

---

[1] R. K. Puri, P. Chattopadhyay, and R. K. Gupta, Phys. Rev. C **43**, 315 (1991).

[2] R. K. Puri and R. K. Gupta, J. Phys. G: Nucl. Part. Phys. **17**, 1933 (1991).

[3] R. K. Puri and R. K. Gupta, J. Phys. G: Nucl. Part. Phys. **18**, 903 (1992).

[4] R. K. Puri and R. K. Gupta, Int. J. Mod. Phys. E **1**, 269 (1992).

[5] R. K. Puri and R. K. Gupta, Phys. Rev. C **45**, 1837 (1992).

[6] R. K. Puri and R. K. Gupta, Phys. Rev. C **51**, 1568 (1995).

[7] M. K. Sharma, H. Kumar, R. K. Puri, and R. K. Gupta, Phys. Rev. C **56**, 1175 (1997).

[8] M. K. Sharma, R. K. Puri, and R. K. Gupta, Eur. Phys. J. A **2**, 69 (1998).

[9] R. K. Puri, R. Arora, and R. K. Gupta, Phys. Rev. C **60**, 054619 (1999).

[10] R. Arora, R. K. Puri, and R. K. Gupta, Eur. Phys. J. A **8**, 103 (2000).

[11] D. Vautherin and D. M. Brink, Phys. Rev. C **5**, 626 (1972).

[12] M. K. Sharma, R. K. Puri, and R. K. Gupta, Z. Phys. A **359**, 141 (1997).

[13] R. K. Gupta, M. K. Sharma, and R. K. Puri, Il. Nuovo Cimento **110A**, 1149 (1997).

[14] R. K. Puri, M. K. Sharma, and R. K. Gupta, Eur. Phys. J. A **3**, 277 (1998).

[15] B. Grammaticos and A. Voros, Ann. Phys. (NY) **123**, 359 (1979).

[16] B. Grammaticos and A. Voros, Ann. Phys. (NY) **129**, 153 (1980).

[17] M. Brack, C. Guet, and H.-B. Hakansson, Phys. Rep. **123**, 275 (1985).

[18] J. Bartel and K. Bencheikh, Eur. Phys. J. A **14**, 179 (2002).

[19] V. Yu. Denisov and W. Nörenberg, Eur. Phys. J. A **15**, 375 (2002).

[20] A. Dobrowolski, K. Pomorski, and J. Bartel, Nucl. Phys. **A729**, 713 (2003).

[21] N. Wang, E. Zhao, Z. Li, X. Wu, M. Liu, J. Li, and W. Scheid, in *Proceedings of the Workshop on Superheavy Elements*, Rauischholzhausen, 6 September 2005 (ISBN 3-00-017194-0) edited by N. V. Antonenko and W. Scheid, Giessen 2005 (Institute für Theoretische Physik, J.-L.-Univerität, Giessen, Germany), p. 115; M. Liu, N. Wang, Z. Li, X. Wu, and E. Zhao, Nucl. Phys. **A768**, 80 (2006).

[22] J. Bartel, M. Brack, and M. Durand, Nucl. Phys. **A445**, 263 (1985).

[23] D. Singh and R. K. Gupta, *Proceedings of DAE-BRNS Symposium on Nuclear Physics*, Mumbai, India, 2003, Vol. **B46**, p. 254.

[24] U. Mosel, P.-G. Zint, and K. H. Passler, Nucl. Phys. **A236**, 252 (1974).

[25] R. K. Gupta, M. K. Sharma, S. Singh, R. Nouicer, and C. Beck, Phys. Rev. C **56**, 3242 (1997).

[26] M. K. Sharma, R. K. Gupta, and W. Scheid, J. Phys. G: Nucl. Part. Phys. **26**, L45 (2000).

[27] R. K. Gupta, M. Balasubramaniam, C. Mazzocchi, M. La Commara, and W. Scheid, Phys. Rev. C **65**, 024601 (2002).

[28] W. Myers and W. J. Swiatecki, Nucl. Phys. **A81**, 1 (1966).

[29] P. Möller, J. R. Nix, W. D. Myers, and W. J. Swiatecki, At. Data Nucl. Data Tables **59**, 185 (1995).

[30] N. J. Davidson, S. S. Hsiao, J. Markram, H. G. Miller, and Y. Tzeng, Nucl. Phys. **A570**, 61c (1994).

[31] M. Balasubramaniam, R. Kumar, R. K. Gupta, C. Beck, and W. Scheid, J. Phys. G: Nucl. Part. Phys. **29**, 2703 (2003).

[32] R. K. Gupta, M. K. Sharma, N. V. Antonenko, and W. Scheid, J. Phys. G: Nucl. Phys. **25**, L47 (1999).

[33] R. R. Betts, *Proceedings of the Conference on Resonances in Heavy Ion Reactions, Bad Hönnef: Lecture Notes in Physics, Vol. 156*, edited by K. A. Eberhardt (Springer, Berlin, 1981), p. 185.

[34] R. R. Betts, *Proceedings of the 5th Adriatic International Conference on Nuclear Physics, Hvar, Croatia, Yugoslavia: Fundamental Problems in Heavy on Collisions*, edited by N. Cindro *et al.* (World Scientific, Singapore, 1984), p. 33.

[35] A. T. Hasan, S. J. Sanders, K. A. Farrar, F. W. Prosser, B. B. Back, R. R. Betts, M. Freer, D. J. Henderson, R. V. F. Janssens, A. H. Wuosmaa, and A. Szanto de Toledo, Phys. Rev. C **49**, 1031 (1994).

[36] K. A. Farrar, S. J. Sanders, A. K. Dummer, A. T. Hasan, F. W. Prosser, B. B. Back, I. G. Bearden, R. R. Betts, M. P. Carpenter, B. Crowell, M. Freer, D. J. Henderson, R. V. F. Janssens, T. L. Khoo, T. Lauritsen, Y. Liang, D. Nisius, A. H. Wuosmaa, C. Beck, R. M. Freeman, Sl. Cavallaro, and A. Szanto de Toledo, Phys. Rev. C **54**, 1249 (1996).

[37] W. Scheid, R. Ligensa, and W. Greiner, Phys. Rev. Lett. **21**, 1479 (1968).

[38] D. Singh and R. K. Gupta, Phys. Rev. C (2007), in process.

[39] D. M. Brink and Fl. Stancu, Nucl. Phys. **A299**, 321 (1978).

[40] P. Chattopadhyay and R. K. Gupta, Phys. Rev. C **30**, 1191 (1984).

[41] P. Bonche and D. Vautherin, Nucl. Phys. **A372**, 496 (1981).

[42] L. R. B. Elton, *Nuclear Sizes* (Oxford University Press, London, 1961).

[43] H. de Vries, C. W. de Jager, and C. de Vries, At. Data Nucl. Data Tables **36**, 495 (1987).

[44] S. Shlomo and J. B. Natowitz, Phys. Rev. C **44**, 2878 (1991).

[45] J. Blocki, J. Randrup, W. J. Swiatecki, and C. F. Tsang, Ann. Phys. (NY) **105**, 427 (1977).